THE JOURNAL OF BIOLOGICAL CHEMISTRY VOL. 287, NO. 50, pp. 42373–42378, December 7, 2012

Electron Microscopic Analysis of a Spherical Mitochondrial Structure*[S]

Received for publication, August 25, 2012, and in revised form, October 12, 2012 Published, JBC Papers in Press, October 23, 2012, DOI 10.1074/jbc.M112.413674

Wen-Xing Ding[‡1], Min Li[§], Joanna M. Biazik[¶], David G. Morgan[‖], Fengli Guo[**], Hong-Min Ni[‡], Michael Goheen[§], Eeva-Liisa Eskelinen[¶], and Xiao-Ming Yin[§2]

From the [‡]Department of Pharmacology, Toxicology, and Therapeutics, the University of Kansas Medical Center, Kansas City, Kansas 66160, the [§]Department of Pathology and Laboratory Medicine, Indiana University School of Medicine, Indianapolis, Indiana 46202, the [¶]Department of Biosciences, Division of Biochemistry and Biotechnology, the University of Helsinki, 00014 Helsinki, Finland, the [‖]Cryo-Transmission Electron Microscopy Facility, Indiana University, Bloomington, Indiana 47405, and the [**]Stowers Institute for Medical Research, Kansas City, Missouri 64110

Background: Mitochondria are dynamic organelles with variable morphological features under different functional status.
Results: Mitochondria treated with an uncoupler presented a spherical structure with an internal lumen containing cytosolic materials as defined by serial sections and electron tomography.
Conclusion: Mitochondria were able to undergo a three-dimensional structural transformation under oxidative stress.
Significance: Mitochondrial spheroid formation represents a novel mitochondrial dynamics.

Mitochondria undergo dynamic structural alterations to meet changing needs and to maintain homeostasis. We report here a novel mitochondrial structure. Conventional transmission electron microscopic examination of murine embryonic fibroblasts treated with carbonyl cyanide *m*-chlorophenylhydrazone (CCCP), a mitochondrial uncoupler, found that more than half of the mitochondria presented a ring-shaped or C-shaped morphology. Many of these mitochondria seemed to have engulfed various cytosolic components. Serial sections through individual mitochondria indicated that they formed a ball-like structure with an internal lumen surrounded by the membranes and containing cytosolic materials. Notably, the lumen was connected to the external cytoplasm through a small opening. Electron tomographic reconstruction of the mitochondrial spheroids demonstrated the membrane topology and confirmed the vesicular configuration of this mitochondrial structure. The outside periphery and the lumen were defined by the outer membranes, which were lined with the inner membranes. Matrix and cristae were retained but distributed unevenly with less being kept near the luminal opening. Mitochondrial spheroids seem to form in response to oxidative mitochondrial damage independently of mitophagy. The structural features of the mitochondrial spheroids thus represent a novel mitochondrial dynamics.

Mitochondria are dynamic organelles, exhibiting changes in size, morphology, mobility, localization, and turnover, which are intimately associated with adaptive and functional alterations, quality control, and homeostasis (1–3). Mitochondria participate in key cellular functions and in turn affect aging, tumorigenesis, neurodegeneration, and oxidative tissue injury (2–7). These conditions can also cause mitochondria damage, which in turn further exacerbates disease progression via the increased production of reactive oxygen species.

Mitochondria are delimited by double membranes, enclosing the matrix compartment that contains the mitochondrial DNA. The topology of the inner membrane is dynamically controlled, hence the greater variation in the morphology of the cristae. The outer membrane does not present such variations but set the boundary for the organelle. Another morphological aspect of the mitochondrial dynamics involves the change in size through the fission and fusion process. Abnormality in this process can lead to the formation of giant or fragmented mitochondria, respectively (2, 3).

Carbonyl cyanide *m*-chlorophenylhydrazone (CCCP)[3] is a reversible mitochondria uncoupler. CCCP rapidly causes mitochondrial depolarization and fragmentation, which can in turn broadly affect mitochondrial functions and trigger multiple responses (3, 8). Here we report that CCCP can trigger a unique form of mitochondrial dynamic process, which is characterized by a distinct structural transformation. This allows the formation of a spherical mitochondrion, here called a mitochondrial spheroid, which enwraps cytoplasm and other organelles. Electron serial sectioning and tomographic studies indicate that these structures were nearly completely delimited, with only a small orifice present that connects the lumen to the cytosol. The unique structure represents a novel mitochondrial dynamics.

* This work was supported, in whole or in part, by National Institutes of Health Grants R01 AA020518-01, R21AA017421, P20 RR021940, and P20 RR016475 (to W.-X. D.) and R01CA111456 and R01CA 83817 (to X.-M. Y.).
[S] This article contains supplemental Fig. S1 and Videos 1–5.
[1] To whom correspondence may be addressed: Dept. of Pharmacology, Toxicology, and Therapeutics, The University of Kansas Medical Center, MS 1018, 3901 Rainbow Blvd., Kansas City, KS 66160. Tel.: 913-588-9813; Fax: 913-588-7501; E-mail: wxding@kumc.edu.
[2] To whom correspondence may be addressed: Dept. of Pathology and Laboratory Medicine, Indiana University School of Medicine, W. 350 11th Street, Indianapolis, IN 46202. Tel.: 317-491-6096; Fax: 317-274-1782; E-mail: xmyin@iupui.edu.

[3] The abbreviations used are: CCCP, carbonyl cyanide *m*-chlorophenylhydrazone; IIM, inside inner membranes; IOM, inside outer membranes; MEF, murine embryonic fibroblast; OIM, outside inner membranes; OOM, outside outer membranes.

EXPERIMENTAL PROCEDURES

Chemicals and Antibodies—CCCP was obtained from Sigma-Aldrich. Anti-Tom20 was from Santa Cruz Biotechnology (Santa Cruz, CA). The secondary antibody for immuno-EM was conjugated with 5-nm gold particles (GE Healthcare).

Cell Lines and Cell Culture—Murine embryonic fibroblasts (MEFs) were maintained in DMEM with 10% fetal bovine serum (GIBCO) supplemented with L-glutamine, and penicillin/streptomycin. Cells were treated with CCCP (30 μM) for 6 h unless otherwise indicated in the figure legends.

Conventional Electron Microscopy—Cells were fixed in 2.5% glutaraldehyde in 0.1 M phosphate buffer (pH 7.4), followed by 1% OsO_4. Sections were examined with a JEM 1011CX electron microscope (JEOL, Peabody, MA). Images were acquired digitally.

Immunoelectron Microscopy—Cells were fixed in 2% paraformaldehyde/0.01% glutaraldehyde in PBS. Cells were pelleted in 3% gelatin in PBS and solidified on ice. Small blocks (~0.5 mm) of the cell pellet were prepared and infiltrated with 2.3 M sucrose at 4 °C overnight. Blocks were mounted on aluminum stubs, frozen, and sectioned. The sections (60 nm) were picked up in drops of 2.3 M sucrose and collected on Formvar-coated mesh grids. After blocking in 1% BSA in PBS the sections were incubated with a primary rabbit anti-Tom20 antibody and subsequently incubated with a secondary antibody conjugated with 5-nm gold particles. The sections were fixed in 1% glutaraldehyde and stained with ice-cold 0.4% uranyl acetate/1% methyl cellulose (pH 4) and dried. The samples were viewed in a Tecnai transmission electron microscope (FEI, Hillsboro, OR).

Serial Section EM—Serial sections (50 nm thick) were collected onto copper slot grids and poststained in 2% uranyl acetate and lead citrate. Images were acquired using a Tecnai 12 transmission electron microscope (Philips Electron Optics, Holland) operating at 80 kV. Mitochondrial membranes were traced by hand, and Amira software (Visage Imaging Inc.) was used to create three-dimensional models of the mitochondrial structures.

Electron Tomography—250–300-nm sections were picked up on 2 × 1-mm copper slot grids with a 50-nm thick LUXFilm™ support film (Ted Pella, Inc.). The grids were stained with 3% uranyl acetate (aq.) followed by Reynolds lead citrate prior to electron microscopic examination. Images were acquired using a JEM 3200FS electron microscope (JEOL) and the HTR (high tilt) specimen holder (JEOL). All tilt series were recorded over the tilt range of approximately ±60° using the automated tilt series collection program serialEM (9). The thickness of each tomography slice is estimated to be 2–3 nm. Tomograms were generated using IMOD (10). For the work presented here, we used either 15-nm colloidal gold fiducials or local patch tracking to align the images prior to three-dimensional reconstruction. Membrane boundaries were manually marked and rendered in the third dimension using IMOD.

RESULTS

CCCP Induces Mitochondrial Spheroids—CCCP has been widely used to study a Parkin-dependent mitophagy process (11–17). CCCP does not induce any significant levels of mitophagy in MEFs because the level of Parkin was below the detection in these cells (13, 17). Unexpectedly, electron microscopy could readily detect ring-shaped structures (Fig. 1*A*). They were not autophagosomes but were identified with typical mitochondrial features, including the double membranes and the cristae. It seemed that a portion of the mitochondrion was compressed, and the loss of the cristae and the matrix at that part allowed the membrane to bend around cytosolic constituents to form a spherical structure (Fig. 1*B*). These structures could be detected after only 1 h of treatment, reaching the plateau between 6 and 16 h and declining at 24 h (27).

Immuno-EM analysis with an antibody against a mitochondrial outer membrane protein, Tom20, found the signals present in both the outside and inside of the vesicular structure (Fig. 1*C*), further confirming their mitochondrial origin and the topological evolution. Various cytoplasmic components, including the cytosol, membranes, vesicles and even another mitochondrion, could be found in the engulfing mitochondria (Fig. 1*B*), suggesting that they could be nonselectively enclosed by the extended mitochondrial membranes during the formation of the spherical structure. As such, these structures were operationally named mitochondrial spheroids although it is not clear whether the enclosed materials were actively or passively engulfed by the mitochondria.

Ring-shaped mitochondrial structures had been reported in early studies based on either fluorescence microscopy (18–21) or electron microscopy (22–26). It was possible that the mitochondrial structure described here could simply reflect a fusion between two ends of a mitochondrion, as suggested by many of these studies. To determine whether this was the case, we performed serial sections for EM examination.

Through the analysis of a total of 22 ring-shaped mitochondria with serial sections, we found that they actually represented spherical structures that were mostly delimited (Fig. 2 and supplemental Fig. S1, *A* and *B*). Thus, the structure was not simply formed by a simple fusion between two parts of a mitochondrion, resulting in a "donut," but rather involved a three-dimensional transformation of the entire mitochondrion, forming a clearly defined internal space surrounded by the mitochondrial membranes. Interestingly, in all of such structures analyzed, there was a small orifice present in the spherical structure. This seemed to provide a pathway connecting the internal space, or the lumen, to the cytoplasm. No similar configurations had been found in a regular mitochondrion (supplemental Fig. S1*C*).

Electron Tomography Reveals the Membrane Topology of the Mitochondrial Spheroids—To further understand the topological relationship of the membranes that form the mitochondrial spheroids, we conducted electron tomography. Shown in Fig. 3*A* and supplemental Video 1 are three examples of mitochondrial spheroids, among which two were subjected to reconstruction (Fig. 3, *B* and *C*, and supplemental Videos 2 and 3). The reconstruction indicated that the vesicular lumen was formed by the original outer membranes, now termed the inside outer membranes (IOM). The peripheral boundary of the mitochondrial spheroids was still defined by the outer membranes, now termed the outside outer membranes (OOM). OOM and IOM connected to each other due to the presence of the orifice, which was surrounded by these membranes. As such, the luminal contents could have exchanges with the cytoplasm.

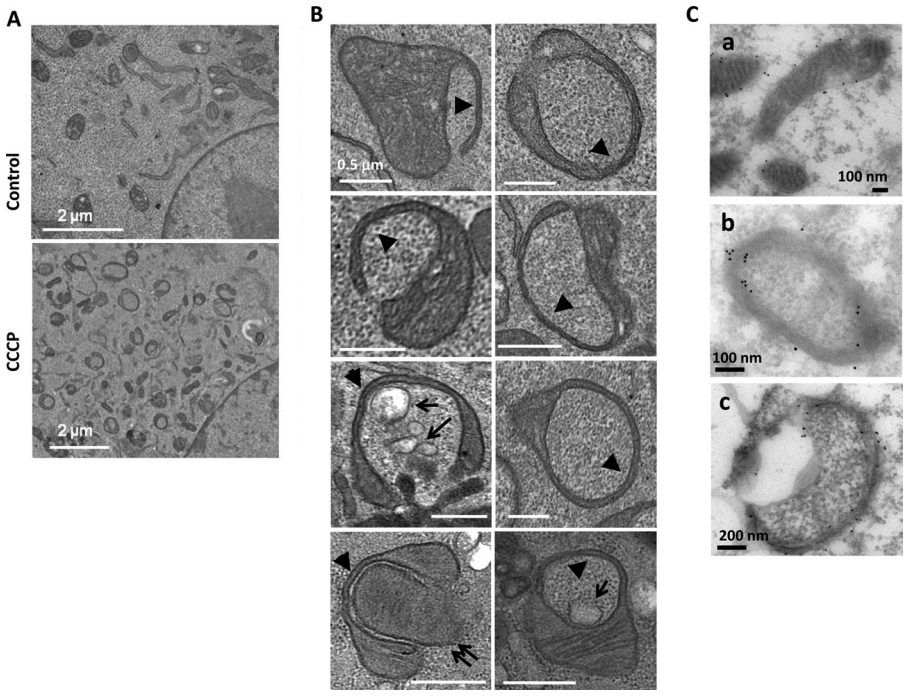

FIGURE 1. **CCCP induces mitochondrial spheroid formation.** *A*, control or MEFs treated with CCCP for 6 h were fixed and subjected to EM examination. CCCP induced a significant level of ring-shaped mitochondria in MEFs. *B*, features of ring-shaped mitochondria induced by CCCP included the compression of a portion of the mitochondria to form a quadruple-membrane segment (*arrowheads*), which seemed to allow the bending of the membrane to circle around cytoplasmic components. These subcellular materials included the cytosol, vesicles (*arrows*), or a mitochondrion (*double arrows*). *C*, wild type MEFs treated with CCCP for 6 h were processed for immuno-EM with anti-Tom20. *a*, normal mitochondria; *b* and *c*, mitochondrial spheroids. The gold particles indicated the Tom20 signals and were present in both the inside and outside of the ring-shaped mitochondria (*b* and *c*), suggesting the presence of mitochondrial outer membranes at these locations.

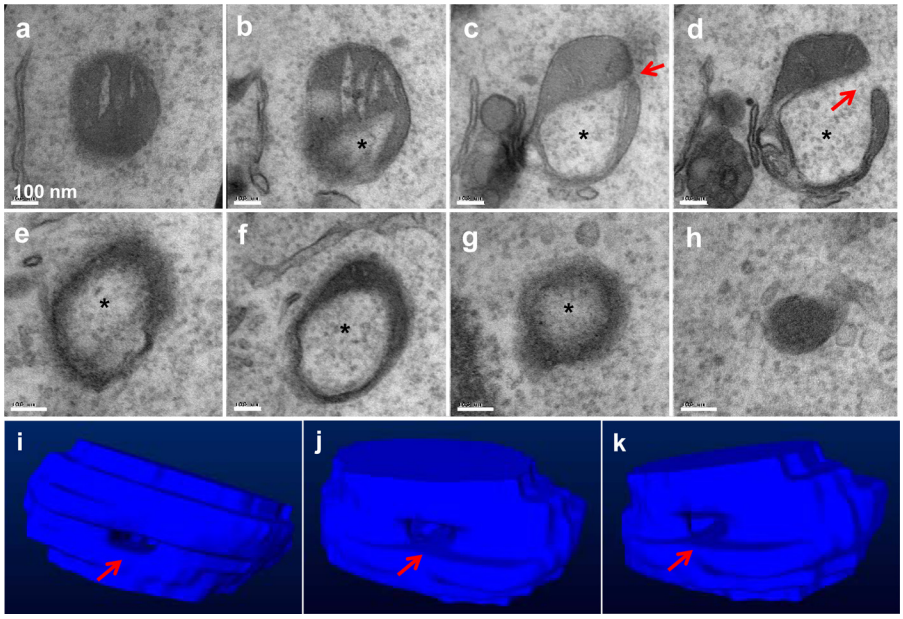

FIGURE 2. **Serial sections of a mitochondrial spheroid.** MEFs treated with CCCP for 6 h were fixed for EM examination. When areas enriched for the mitochondrial spheroids were identified, serial sections were performed. Shown in *a*–*h* is a series of sections separated by 50 nm in distance. Note the lumen (*asterisk*) that contains the cytosol and the orifice (*arrow*) that connects the lumen to the cytoplasm. The serial sections allowed the construction of a three-dimensional model, and representative views of the model are shown in *i*–*k*.

Not depicted in Fig. 3, *B* and *C*, but in Fig. 4 and supplemental Videos 4 and 5 were the original inner membranes, which were lined against the inside and outside outer membranes, and could thus also be categorized as inside inner membranes (IIM) and outside inner membranes (OIM) (Fig. 4). Between the membranes the matrix and the cristae were redistributed nonsymmetrically with certain parts left with membranes only (Figs. 3 and 4). Mitochondrial matrix could be defined in a portion of the mitochondrial spheroid between IIM and OIM, but not in other part of the structure, which was bordered by only four layers of membranes (IOM, IIM, OIM and OOM) (Fig. 1*B*). Cristae were readily identi-

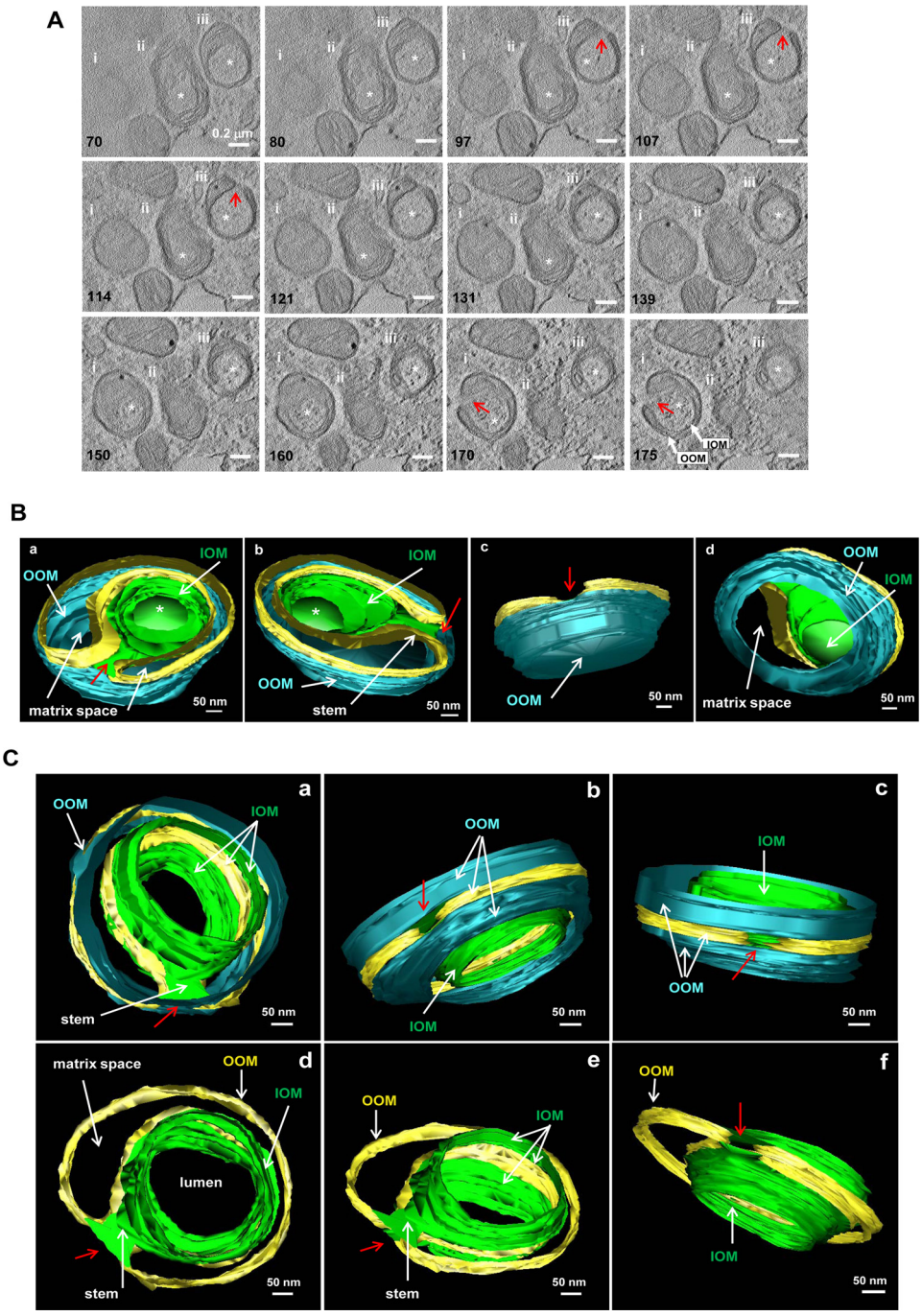

FIGURE 3. **Electron tomography of mitochondrial spheroids.** MEFs treated with CCCP for 6 h were fixed and subjected to electron tomography. The topographic slices (*A*) illustrate three mitochondrial spheroids (*i*, *ii*, and *iii*), from which the three-dimensional models of spheroids *i* (*B*) and *iii* (*C*) were reconstructed. Images were extracted from supplemental Videos 1–3. Only the outer membrane was traced and modeled. The *numbers* in *A* represent those of slices along the *z* axis of the original volume. The lumen of the spheroid (indicated by an *asterisk* in *A*) was delimited by the inside outer membranes (IOM, *green*) and opened to the cytoplasm through an orifice (*red arrows*). The outside outer membrane (OOM, *cyan*) was the same OM that extended to the IOM, and the relationship is indicated by the *gold-colored strip*. IOM and OOM were linked by a membranous stem that embedded the orifice (*C*). Between IOM and OOM were the inner membranes (not depicted in the model) and the matrix space (indicated, *B* and *C*). The model in *B* also showed that the spheroid and its internal lumen were completely delimited at one end that was preserved in this volume. Removal of the OOM at this end allowed the visualization of the delimited lumen from the matrix side (*Bd*). The model in *C* also illustrates the connection of the lumen to the cytoplasm by the orifice, which was embedded in a membranous stem. Part of the OOM was removed for a clearer view (C, *d–f*).

fied in the matrix space (Fig. 4). They remained the lamellar form and were contiguous to the inner membranes. Overall, the electron tomography gave rise to a clear depiction of the spherical nature and membrane topology of the mitochondrial spheroid.

DISCUSSION

Mitochondrial spheroids can manifest as ring-shaped mitochondria on conventional transmission EM (Fig. 1). Many studies, using EM (18, 22–26 and references within) or, more recently, fluorescence microscopy (18–21) have described this

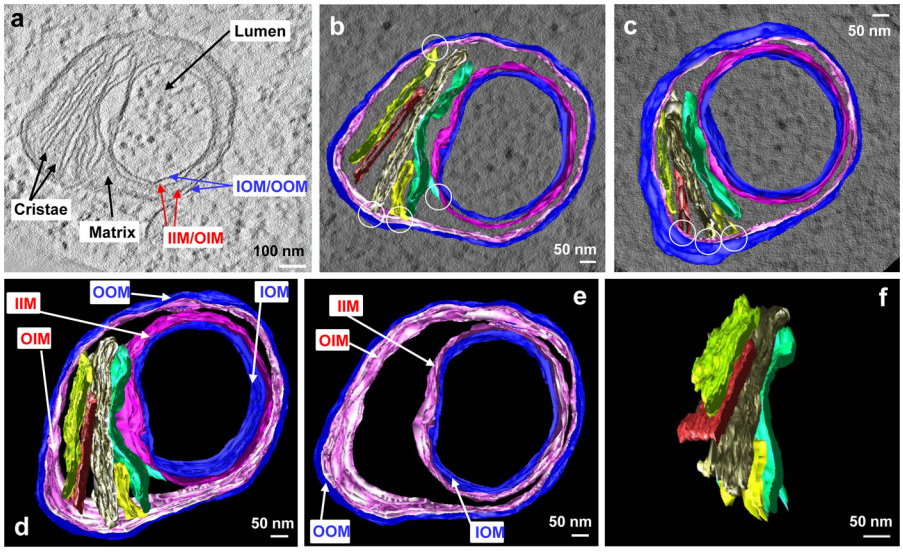

FIGURE 4. **The topological relationship of inner and outer membranes in a mitochondrial spheroid.** *a*, a tomographic slice shows the inner membrane (IM), the outer membrane (OM), and the matrix enclosed by the IM, in which two of the five cristae are also indicated. *b–f*, the three-dimensional model of the IM (*magenta*), the OM (*blue*) and the five cristae (in various colors) were superimposed on a tomographic slice and viewed from the top (*b*) and bottom (*c*). Note the connection of the cristae to the IM (*white circles*). *d–f* show the model with all of the membrane components (*d*), the IM and OM only (*e*), and the cristae only (*f*). Note the lamellar form of the cristae in *f*. Images *a* and *b–f* were extracted from supplemental Videos 4 and 5, respectively.

type of mitochondria in very diverse cellular contexts. However, the actual morphology can vary significantly, and it is not clear whether the same subcellular phenomenon had been investigated in these cases. This is particularly true when the description of the mitochondrial morphology is based solely on fluorescence microscopy. Hence different mechanisms could account for the similar but not necessarily exact morphological changes of the mitochondria under these scenarios. Whereas the ring-shaped mitochondria could be found in apparently normal tissues (22, 24, 26), they are also frequently identified in stress conditions (18–21, 23). Our studies presented in this, and a companion paper (27) represents the latter condition, which suggests that mitochondria can undergo active conversion between the normal morphology and the ring-shaped morphology.

This conversion may be due to end-to-end or end-to-side fusion of elongated mitochondria at two-dimensional level, forming donut-shaped mitochondria as suggested by some of the studies (18, 21, 26). Alternatively, this conversion can represent a vesicle-like structure with a lumen surrounded by the mitochondrial membranes, as supported by the present study. We have also structurally identified the presence of a pore, which would allow the cytoplasm trapped in the lumen to be confluent with the external cytoplasm. However, it is not clear whether this represents an incomplete fusion of the membrane or an integrated part of the structural feature. The significance of such a pore is thus unknown at this time. Our model is supported by both serial sections and tomographic reconstruction. It would be also supported by two earlier studies where serial sections were performed (24, 26) and a similar pore was observed (24).

Electron tomography further reveals the membrane topology that may explain how the spherical structure is formed. Mitochondrial spheroid formation would require the extension of the mitochondrial membranes to bend around the cytoplasm to form a new spherical structure with an internal lumen, in which cytosolic materials are likely trapped nonspecifically (Figs. 1 and 2). The revelation of these three-dimensional features provides the rationale to categorize this mitochondrial structure in its own group. The morphology of the mitochondrial spheroid looks almost like a phagosome in the sense that the spherical structure enwraps the cytosolic contents in the internal space. However, whether this transformation may involve any molecular events similar to the membrane dynamics responsible for phagocytosis (as in heterophagosome or autophagosome formation) is not known.

We have investigated several molecular mechanisms that could be involved in the formation of the spherical mitochondria following CCCP treatment (27). The autophagy machinery does not seem to be required, but reactive oxygen species and mitofusins are required. In addition, Parkin serves as a negative regulator by promoting mitofusin degradation. Mitofusins are known to function in mitochondrial tethering and fusion. Thus mitofusins can be equally important in the self-fusion of the mitochondrial membrane during the formation of mitochondrial spheroid. However, there would likely be other molecular events to affect the membrane curvature for such a process to initiate and to complete. In particular, mechanisms for curvature and branching of filamentous mitochondria are little understood, and they could be conceivably involved in the formation of mitochondrial spheroids.

The significance of the mitochondrial spheroids has yet to be fully determined. Common autophagy inducers, such as starvation and endoplasmic reticulum stress, did not induce mitochondrial spheroids. CCCP can induce oxidative mitochondrial damage. Another inducer of mitochondrial spheroids, sodium azide, is also a mitochondrial toxin (27). An earlier study (23) found this type of mitochondria in the livers of rat given long term alcohol diet. Furthermore, we had found that acetaminophen at a dose that induces significant oxidative mitochondrial

damage, also induced mitochondrial spheroids in hepatocytes *in vivo* (27). In both CCCP and acetaminophen cases, antioxidants could prevent mitochondrial spheroid formation. Finally, the number of these spherical mitochondria increased with age in retinal pigment epithelium in birds, which may be related to long term light stimulation (26). It is thus tempting to suggest that this type of mitochondrial dynamics could be involved in pathological conditions that involve mitochondrial oxidative injury.

In a separate study (27) we reported that CCCP-induced mitochondrial spheroids formation can be a reversible process as other CCCP-induced phenomena, such as mitochondrial depolarization, mitochondrial fragmentation, and autophagy induction because all of these changes will disappear when CCCP is removed from the medium. These findings could suggest that once an adverse pathological condition is remedied, this mitochondrial alteration could be reversed.

In conclusion, mitochondrial spheroid formation represents a novel mitochondrial dynamic process that is distinctive from other commonly known dynamics. The formation of such a spherical structure poses challenging questions regarding the membrane dynamics, molecular details and pathophysiological consequences, which need to be resolved in the future.

Acknowledgments—We thank Barbara Fegley (University of Kansas Medical Center Electron Microscopy Research Laboratory) for excellent assistance with the EM studies; Teri Johnson and Ting Xie (Stowers Institute for Medical Research) for support in reagents and facility use; and Ilya Belevich and Helena Vihinen (University of Helsinki) for technical assistance with Amira software.

REFERENCES

1. Scheffler, I. E. (1999) in *Mitochondria* (Scheffler, I. E., ed) pp. 15–47, Wiley-Liss, New York
2. Westermann, B. (2010) Mitochondrial fusion and fission in cell life and death. *Nat. Rev. Mol. Cell Biol.* **11,** 872–884
3. Chan, D. C. (2006) Mitochondria: dynamic organelles in disease, aging, and development. *Cell* **125,** 1241–1252
4. Wallace, D. C., Fan, W., and Procaccio, V. (2010) Mitochondrial energetics and therapeutics. *Annu. Rev. Pathol.* **5,** 297–348
5. Lemasters, J. J. (2005) Selective mitochondrial autophagy, or mitophagy, as a targeted defense against oxidative stress, mitochondrial dysfunction, and aging. *Rejuvenation Res.* **8,** 3–5
6. Green, D. R., Galluzzi, L., and Kroemer, G. (2011) Mitochondria and the autophagy-inflammation-cell death axis in organismal aging. *Science* **333,** 1109–1112
7. Youle, R. J., and Narendra, D. P. (2011) Mechanisms of mitophagy. *Nat. Rev. Mol. Cell. Biol.* **12,** 9–14
8. Ricci, J. E., Waterhouse, N., and Green, D. R. (2003) Mitochondrial functions during cell death, a complex (I-V) dilemma. *Cell Death Differ.* **10,** 488–492
9. Mastronarde, D. N. (2005) Automated electron microscope tomography using robust prediction of specimen movements. *J. Struct. Biol.* **152,** 36–51
10. Kremer, J. R., Mastronarde, D. N., and McIntosh, J. R. (1996) Computer visualization of three-dimensional image data using IMOD. *J. Struct. Biol.* **116,** 71–76
11. Narendra, D., Tanaka, A., Suen, D. F., and Youle, R. J. (2008) Parkin is recruited selectively to impaired mitochondria and promotes their autophagy. *J. Cell Biol.* **183,** 795–803
12. Geisler, S., Holmström, K. M., Skujat, D., Fiesel, F. C., Rothfuss, O. C., Kahle, P. J., and Springer, W. (2010) PINK1/Parkin-mediated mitophagy is dependent on VDAC1 and p62/SQSTM1. *Nat. Cell Biol.* **12,** 119–131
13. Ding, W. X., Ni, H. M., Li, M., Liao, Y., Chen, X., Stolz, D. B., Dorn, G. W., 2nd, and Yin, X. M. (2010) Nix is critical to two distinct phases of mitophagy, reactive oxygen species-mediated autophagy induction and Parkin-ubiquitin-p62-mediated mitochondrial priming. *J. Biol. Chem.* **285,** 27879–27890
14. Matsuda, N., Sato, S., Shiba, K., Okatsu, K., Saisho, K., Gautier, C. A., Sou, Y. S., Saiki, S., Kawajiri, S., Sato, F., Kimura, M., Komatsu, M., Hattori, N., and Tanaka, K. (2010) PINK1 stabilized by mitochondrial depolarization recruits Parkin to damaged mitochondria and activates latent Parkin for mitophagy. *J. Cell Biol.* **189,** 211–221
15. Lee, J. Y., Nagano, Y., Taylor, J. P., Lim, K. L., and Yao, T. P. (2010) Disease-causing mutations in Parkin impair mitochondrial ubiquitination, aggregation, and HDAC6-dependent mitophagy. *J. Cell Biol.* **189,** 671–679
16. Chan, N. C., Salazar, A. M., Pham, A. H., Sweredoski, M. J., Kolawa, N. J., Graham, R. L., Hess, S., and Chan, D. C. (2011) Broad activation of the ubiquitin-proteasome system by Parkin is critical for mitophagy. *Hum. Mol. Genet.* **20,** 1726–1737
17. Yoshii, S. R., Kishi, C., Ishihara, N., and Mizushima, N. (2011) Parkin mediates proteasome-dependent protein degradation and rupture of the outer mitochondrial membrane. *J. Biol. Chem.* **286,** 19630–19640
18. Messerschmitt, M., Jakobs, S., Vogel, F., Fritz, S., Dimmer, K. S., Neupert, W., and Westermann, B. (2003) The inner membrane protein Mdm33 controls mitochondrial morphology in yeast. *J. Cell Biol.* **160,** 553–564
19. Benard, G., Bellance, N., James, D., Parrone, P., Fernandez, H., Letellier, T., and Rossignol, R. (2007) Mitochondrial bioenergetics and structural network organization. *J. Cell Sci.* **120,** 838–848
20. Cui, M., Tang, X., Christian, W. V., Yoon, Y., and Tieu, K. (2010) Perturbations in mitochondrial dynamics induced by human mutant PINK1 can be rescued by the mitochondrial division inhibitor mdivi-1. *J. Biol. Chem.* **285,** 11740–11752
21. Liu, X., and Hajnóczky, G. (2011) Altered fusion dynamics underlie unique morphological changes in mitochondria during hypoxia-reoxygenation stress. *Cell Death Differ.* **18,** 1561–1572
22. Christensen, A. K., and Chapman, G. B. (1959) Cup-shaped mitochondria in interstitial cells of the albino rat testis. *Exp. Cell Res.* **18,** 576–579
23. Kiessling, K. H., and Tobe, U. (1964) Degeneration of liver mitochondria in rats after prolonged alcohol consumption. *Exp. Cell Res.* **33,** 350–354
24. Stephens, R. J., and Bils, R. F. (1965) An atypical mitochondrial form in normal rat liver. *J. Cell Biol.* **24,** 500–504
25. Setoguti, T. (1977) Electron microscopic studies of the parathyroid gland of senile dogs. *Am. J. Anat.* **148,** 65–83
26. Lauber, J. K. (1982) Retinal pigment epithelium: ring mitochondria and lesions induced by continuous light. *Curr. Eye Res.* **2,** 855–862
27. Ding, W. X., Guo, F., Ni, H. M., Bockus, A., Manley, S., Stolz, D. B., Eskelinen, E. L., Jaeschke, H., and Yin, X. M. (October 24, 2012) Parkin and mitofusins reciprocally regulate mitophagy and mitochondrial spheroid formation. *J. Biol. Chem.* **287,** 42379–42388